Received: 25 December 2020 | Revised: 14 February 2021 | Accepted: 15 February 2021

DOI: 10.1111/gtc.12840

ORIGINAL ARTICLE

Genes to Cells WILEY

RNA polymerase II condensate formation and association with Cajal and histone locus bodies in living human cells

Takashi Imada[1] | **Takeshi Shimi**[2,3] | **Ai Kaiho**[4,5] | **Yasushi Saeki**[4] | **Hiroshi Kimura**[1,2,3]

[1]School of Life Science and Technology, Tokyo Institute of Technology, Yokohama, Japan

[2]World Research Hub Initiative, Institute of Innovative Research, Tokyo Institute of Technology, Yokohama, Japan

[3]Cell Biology Center, Institute of Innovative Research, Tokyo Institute of Technology, Yokohama, Japan

[4]Protein Metabolism Project, Tokyo Metropolitan Institute of Medical Science, Tokyo, Japan

[5]Institute for Advanced Life Sciences, Hoshi University, Tokyo, Japan

Correspondence
Hiroshi Kimura, Graduate School of Life Science, Tokyo Institute of Technology, Yokohama, Japan.
Email: hkimura@bio.titech.ac.jp

Funding information
Japan Agency for Medical Research and Development, Grant/Award Number: JP20am0101105; Japan Society for the Promotion of Science, Grant/Award Number: JP17H01417, JP18H05498 and JP18H05527; Core Research for Evolutional Science and Technology, Grant/Award Number: JPMJCR16G1

Communicated by: Chikashi Obuse

Abstract

In eukaryotic nuclei, a number of phase-separated nuclear bodies (NBs) are present. RNA polymerase II (Pol II) is the main player in transcription and forms large condensates in addition to localizing at numerous transcription foci. Cajal bodies (CBs) and histone locus bodies (HLBs) are NBs that are involved in transcriptional and post-transcriptional regulation of small nuclear RNA and histone genes. By live-cell imaging using human HCT116 cells, we here show that Pol II condensates (PCs) nucleated near CBs and HLBs, and the number of PCs increased during S phase concomitantly with the activation period of histone genes. Ternary PC–CB–HLB associates were formed via three pathways: nucleation of PCs and HLBs near CBs, interaction between preformed PC–HLBs with CBs and nucleation of PCs near preformed CB–HLBs. Coilin knockout increased the co-localization rate between PCs and HLBs, whereas the number, nucleation timing and phosphorylation status of PCs remained unchanged. Depletion of PCs did not affect CBs and HLBs. Treatment with 1,6-hexanediol revealed that PCs were more liquid-like than CBs and HLBs. Thus, PCs are dynamic structures often nucleated following the activation of gene clusters associated with other NBs.

KEYWORDS

Cajal body, histone locus body, liquid droplet, live-cell imaging, RNA polymerase II, transcription

1 | INTRODUCTION

Eukaryotic nuclei are highly organized structures comprising chromatin, the nuclear lamina, nucleoli and nuclear bodies (NBs). NBs are phase-separated liquid droplets that contain specific proteins and RNAs (Strom & Brangwynne, 2019; Uversky, 2017). In humans, RNA polymerase II (Pol II) is the main player in transcription and is composed of 12 subunits. In addition to numerous small transcription foci, Pol II can form relatively large phase-separated condensates via the intrinsically disordered C-terminal domain (CTD) of the RPB1, which is the largest subunit that harbors the catalytic activity (Boehning

This is an open access article under the terms of the Creative Commons Attribution-NonCommercial License, which permits use, distribution and reproduction in any medium, provided the original work is properly cited and is not used for commercial purposes.
© 2021 The Authors. *Genes to Cells* published by Molecular Biology Society of Japan and John Wiley & Sons Australia, Ltd.

et al., 2018; Lu et al., 2018). Human Pol II CTD consists of 52 repeats of hepta-amino acids, Tyr–Ser–Pro–Thr–Ser–Pro–Ser. The Tyr, Ser and Thr residues can be phosphorylated, depending on the transcription status. In general, Ser5 and Ser2 become phosphorylated during the initiation and elongation of transcription, respectively (Harlen & Churchman, 2017; Maita & Nakagawa, 2020). Thus, transcribing Pol II molecules on most of protein coding genes harbor phosphorylated Ser2 (S2P) at the CTD, but those on histone genes and small nuclear RNA (snRNA) genes are only phosphorylated at Ser5 (S5P) (Medlin et al., 2005). Pol II on snRNA genes also harbors phosphorylated Ser7 (S7P) (Egloff et al., 2007, 2012). Phosphorylation of CTD was recently reported to regulate phase separation or condensation of Pol II clusters. Pol II with hypophosphorylated CTD forms clusters with mediators, while Pol II with hyperphosphorylated CTD is clustered with splicing factors (Guo et al., 2019). Pol II large condensates [hereafter termed Pol II condensates (PCs) to avoid confusion with numerous smaller clusters] contain both unphosphorylated and S5P CTD forms (Alm-Kristiansen et al., 2008; Guglielmi et al., 2013; Nizami et al., 2010; Schul et al., 1998; Xie & Pombo, 2006).

Pol II condensates were reported to associate with NBs, such as Cajal/coiled bodies (CBs) and histone locus bodies (HLBs) (Alm-Kristiansen et al., 2008; Guglielmi et al., 2013; Lamond & Carmo-Fonseca, 1993; Nizami et al., 2010; Schul et al., 1998; Xie & Pombo, 2006). CBs are involved in transcriptional and post-transcriptional regulation of histone genes, snRNA genes and small nucleolar RNA (snoRNA) genes via genome organization (Wang et al., 2016; Sawyer et al., 2016), small nuclear ribonucleoprotein (snRNP) biogenesis (Staněk, 2017) and telomerase RNA modification (Henriksson & Farnebo, 2015; Venteicher et al., 2009). CBs tend to localize near sn/snoRNA genes (U1 and U2 snRNA gene arrays on chromosomes 1 and 17, respectively) and *HIST2* locus (six histone genes on chromosome 1) in human cells (Duronio & Marzluff, 2017; Frey & Matera, 2001; Nizami et al., 2010a, 2010b; Shopland et al., 2001; Wang et al., 2016). CBs contain various proteins, such as coilin, survival motor neuron protein (SMN) (Raimer et al., 2016) and telomerase Cajal body protein 1 (TCAB1; also known as WDR79 or WRAP53β) (Henriksson & Farnebo, 2015; Venteicher et al., 2009). Coilin is a marker protein of CBs, and its depletion leads to loss of CBs (Machyna et al., 2015). SMN and TCAB1 contribute to snRNP recycling and telomere maintenance, respectively (Henriksson & Farnebo, 2015; Raimer et al., 2016; Venteicher et al., 2009). SMN is also a component of another, coilin-negative NB called Gem (gemini of Cajal bodies), which is often co-localized with a CB (Cauchi, 2010; Liu & Dreyfuss, 1996; Sleeman et al., 2003). Diverse biological functions of coilin or CBs have been observed during development and reproduction. Coilin-knockout (KO) mice show semi-embryonic lethality and are defective in fertility and fecundity (Tucker et al., 2001; Walker et al., 2009), and coilin-knockdown (KD) zebrafish were embryonic lethal because of insufficient snRNP production (Strzelecka et al., 2010). At the cellular level, coilin-KO mouse and coilin-KD human cells are viable but show impaired splicing efficiency and fidelity, decreased transcription of histone and sn/snoRNA genes, and decreased cell proliferation (Lemm et al., 2006; Tucker et al., 2001; Wang et al., 2016; Whittom et al., 2008). Coilin is considered to play a role as glue to co-assemble many proteins and RNAs into CBs and to facilitate RNP biogenesis (Klingauf et al., 2006).

The HLB is another type of NB that localizes near replication-dependent histone gene loci, such as *HIST1* (55 histone genes on chromosome 6) and *HIST2* (six histone genes on chromosome 1) in humans (Duronio & Marzluff, 2017; Marzluff et al., 2002; Nizami et al., 2010a, 2010b; Wang et al., 2016). HLBs are often found adjacent to CBs, consistent with the association between CBs and *HIST2* (Duronio & Marzluff, 2017; Nizami et al., 2010a, 2010b). HLBs contain proteins essential for both the initiation of histone gene transcription and 3′ cleavage of nonpolyadenylated histone mRNAs, including an HLB marker protein, nuclear protein of the ataxia telangiectasia-mutated locus (NPAT) (Fruscio et al., 1997; Ghule et al., 2008; Ma et al., 2000; Romeo & Schümperli, 2016; Ye et al., 2003). Disruption of the *NPAT* gene results in early embryonic lethality in mice and halts cell proliferation because of G_0/G_1 arrest (Di Fruscio et al., 1997; Ma et al., 2000; Ye et al., 2003).

Although the liquid droplet nature of NBs has recently been studied intensively (Carmo-Fonseca & Rino, 2011; Sawyer et al., 2019; Shevtsov & Dundr, 2011; Staněk & Fox, 2017), it remains unclear how different NBs associate with each other in living cells. In the present study, time-lapse imaging was employed to examine how three NBs (PCs, CBs and HLBs) are formed and interact with each other in living human cells. PCs were often nucleated at the beginning of S phase near CBs or HLBs, with a preferential association with HLBs. PC–CB–HLB ternary associates were formed via three different pathways. Although CBs were not essential for PC formation, the association of PCs with other NBs was affected. PCs were more sensitive to 1,6-hexanediol (1,6-HD) than CBs and HLBs. Our data combined with previous findings suggest that PCs are dynamic structures, and their nucleation is initiated during activation of gene clusters, facilitated by other NBs.

2 | RESULTS

2.1 | Frequent emergence of PCs at entry of S phase in living cells

To examine when and where PCs are formed in living cells, we knocked-in the enhanced green fluorescent protein (EGFP) into both alleles of RPB1 gene in human colon

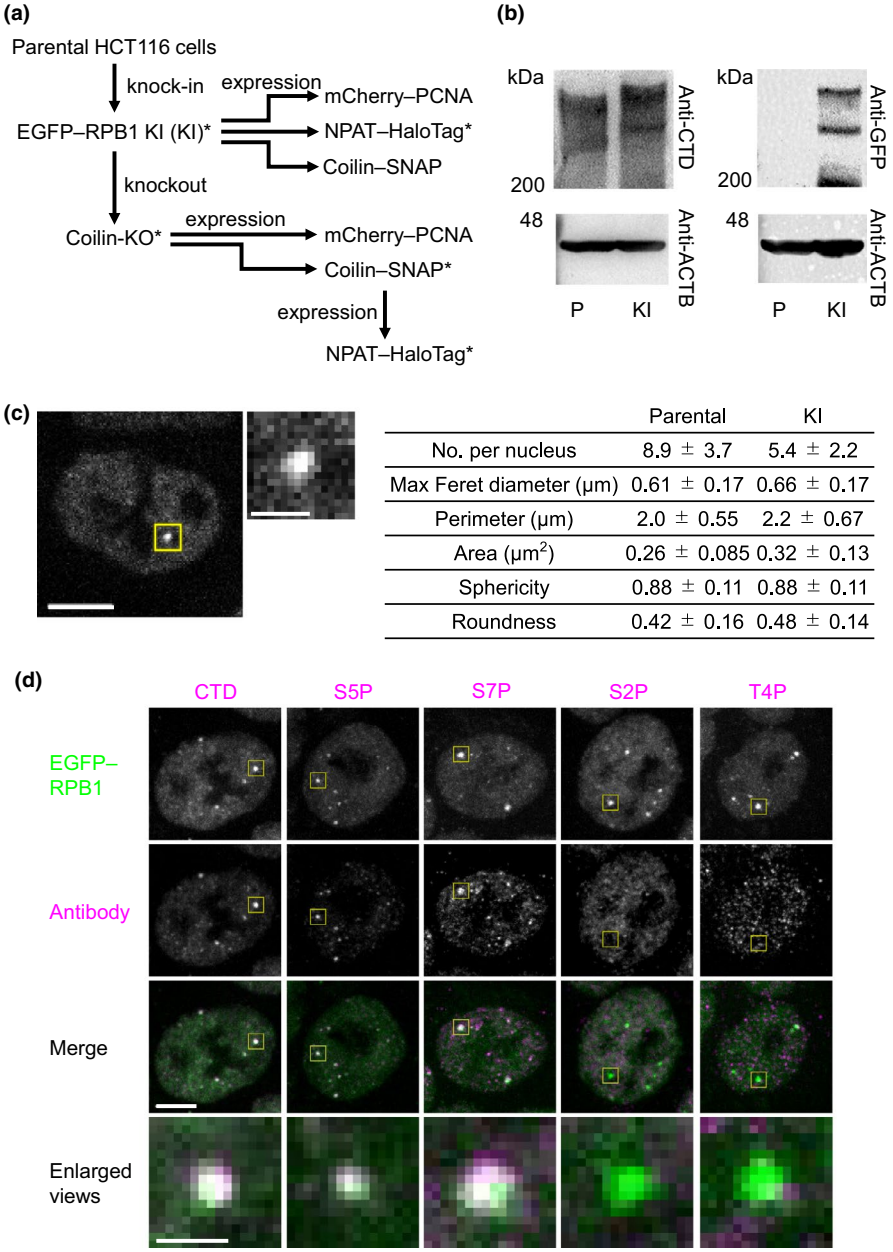

	Parental	KI
No. per nucleus	8.9 ± 3.7	5.4 ± 2.2
Max Feret diameter (μm)	0.61 ± 0.17	0.66 ± 0.17
Perimeter (μm)	2.0 ± 0.55	2.2 ± 0.67
Area (μm^2)	0.26 ± 0.085	0.32 ± 0.13
Sphericity	0.88 ± 0.11	0.88 ± 0.11
Roundness	0.42 ± 0.16	0.48 ± 0.14

FIGURE 1 Generation of EGFP–RPB1 KI cells and characterization of PCs. (a) Summary of the cell lines used in the present study. EGFP–RPB1 KI (KI) is a cell line in which EGFP is knocked-in into both RPB1 alleles and all RPB1 is EGFP-tagged. Asterisks indicate cell lines obtained via single-cell cloning. (b) Western blots. Whole-cell lysates prepared from parental HCT116 (P) and KI (KI) cells were separated and probed with antibodies against Pol II CTD (CMA601), GFP and beta-actin (ACTB). Two bands above 200 kDa on anti-CTD and anti-GFP blots represent hyperphosphorylated (top) and unphosphorylated (bottom) forms (Stasevich et al., 2014). An extra band just below 200 kDa in KI cells on anti-GFP blot may be a degraded form (Pol IIb) during sample preparation or in cells (Chapman et al., 2004; Kim & Dahmus, 1989). (c) EGFP–RPB1 in living KI cells. Single confocal section of EGFP–RPB1 and a magnified view of a Pol II condensate (PC) are shown. The table (right) shows the properties of PCs in parental HCT116 and KI cells, detected by immunofluorescence using anti-CTD and by EGFP–RPB1, respectively. Parameters (means of 50 cells) were determined by intensity thresholding and size constraint (see Experimental Procedures section). The numbers of CBs and HLBs in KI cells (2.8 ± 1.3 and 3.3 ± 1.1, respectively; $n = 100$ cells; Figure S2a; Table S1) were similar to those in parental HCT116 cells (2.8 ± 1.2 and 3.5 ± 1.3, respectively; $n = 100$ cells; Figure S2b; Table S1). (d) Immunofluorescence images of EGFP–RPB1 (green) in KI cells with antibodies against Pol II CTD, S2P, T4P, S5P or S7P, and Cy5-conjugated anti-mouse secondary antibodies (magenta). Magnified views of areas indicated by yellow boxes are shown. Max-Intensity-Projection (MIP) images of Z-stack confocal sections at 0.30 μm intervals (31–34 stacks) to cover the entire nucleus are shown. Scale bars, 5 μm; for magnified views, 1 μm

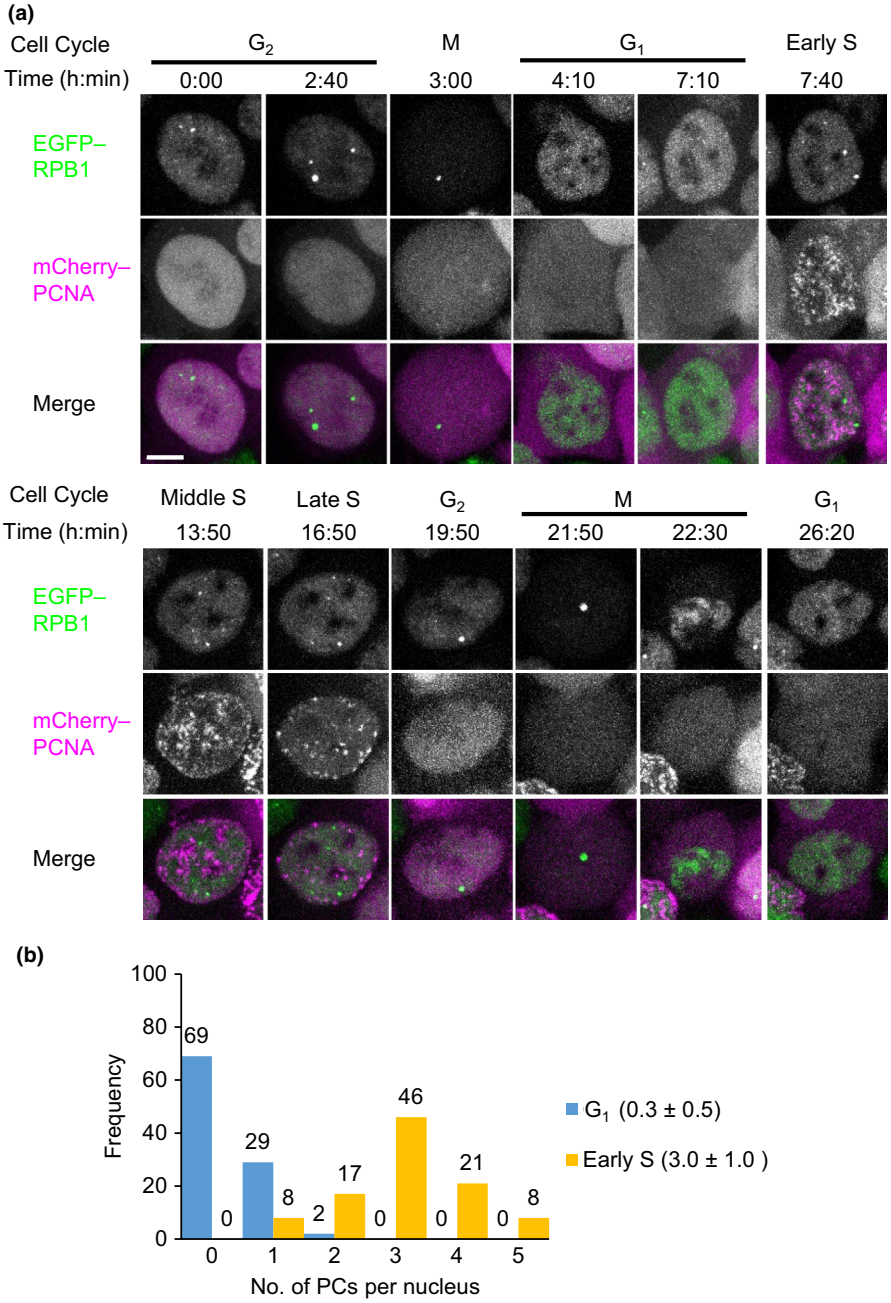

FIGURE 2 PC formation in living cells. (a) Time-lapse images of EGFP–RPB1 and mCherry–PCNA in KI cells expressing mCherry–PCNA. MIP images of 15 Z-stacks at 0.80 μm intervals are shown. (b) Histogram (left) and average ± *SD* (right, $n = 100$ cells) of the number of PCs per nucleus in KI cells in both G_1 and early S phases. Scale bar, 5 μm

cancer HCT116 cells so that EGFP-RPB1 is expressed under the own promotor (Figure 1a). Western blot analysis confirmed that EGFP–RPB1 was expressed in knock-in HCT116 cells (referred as KI cells) at a similar level to that of endogenous RPB1 in wild-type cells (Figure 1b). In living KI cells, EGFP–RPB1 fluorescence was concentrated in several large foci (Pol II condensates or PCs; average 5.4 ± 2.2 per nucleus; range 0–10; Table S1) with a maximum Feret diameter of ~0.7 μm (Figure 1c), as previously reported (Steurer et al., 2018). The number of PCs in living KI cells was slightly lower than that in parental HCT116 cells that were fixed and stained with anti-CTD antibody (average 8.9 ± 3.7 per nucleus; range 0–21). This difference may be due to a higher contrast by immunofluorescence using fixed cells than in living cells where diffuse EGFP–RPB1 is present. The effects of GFP-fusion might also cause the difference; the addition of GFP may partially interfere with the condensate formation and/or may cause CTD truncation as a band below 200 kDa was observed on anti-GFP blot (Figure 1b) (Chapman et al., 2004; Kim & Dahmus, 1989). In this study, however, the 1.6-fold difference in the absolute number had little impact on the analysis and interpretation, as we essentially compared the associations between NBs in KI-derivatives with those in KI cells and the data were supported by immunofluorescence using parental cells. Immunofluorescence using phosphorylation-specific antibodies showed that PCs contained S5P and S7P, but not S2P and T4P, on Pol II CTD

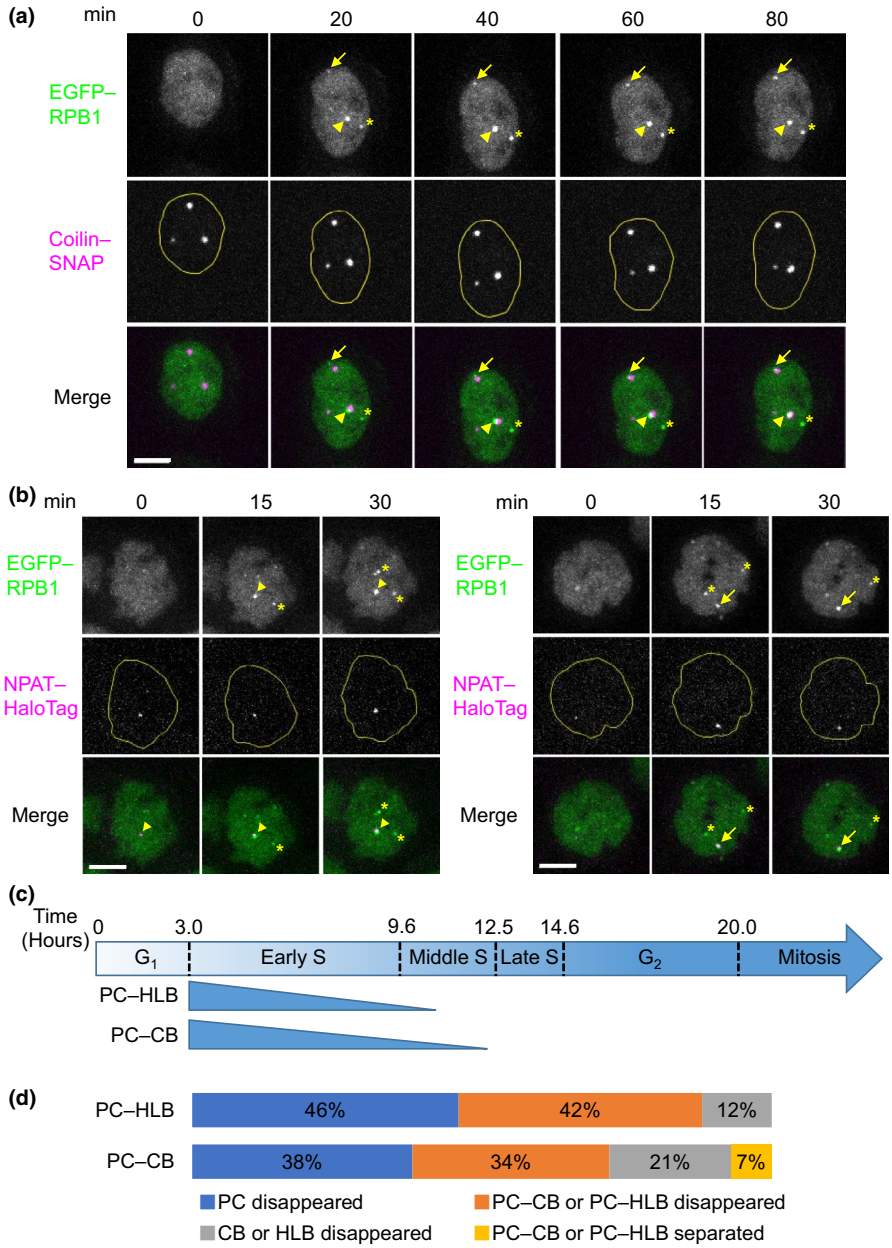

FIGURE 3 PCs nucleated near CBs and HLBs. (a) Time-lapse images of coilin-KO cells expressing coilin–SNAP. Confocal sections for EGFP–RPB1 (Pol II; green in merge) and coilin–SNAP (CBs) labeled with SNAP–Cell 647–SiR (magenta in merge) were acquired. MIP images of 17 Z-stacks at 0.90 μm intervals are shown. A PC nucleated near a CB (arrowhead) and another nucleated apart from a CB (asterisk). A small PC (arrow) became bigger after association with a CB. (b) Time-lapse images of KI cells expressing NPAT–HaloTag. Confocal sections for EGFP–RPB1 (Pol II; green in merge) and NPAT–HaloTag (HLBs) labeled with Janelia Fluor 646 HaloTag ligand (magenta in merge) were acquired. MIP images of 15 Z-stacks at 0.75 μm intervals are shown. A PC (arrowhead) nucleated near an existing HLB and another (asterisk) nucleated apart from an HLB. A PC nucleated with an HLB simultaneously (arrow). Yellow lines indicate nuclear peripheries. (c) Schematic representation of the association between PCs and CBs or HLBs during the cell cycle. PCs nucleated at the entry of S phase (Figure 2a). The majority of PC–CB associates (90%) and PC–HLB associates (76%) dissolved during early S phase. Residual fractions of PC–CB associates (10%) and PC–HLB associates (24%) dissolved by the end of middle S phase (see also Table S3). (d) Dissolution patterns of NB associates (see also Table S3). Scale bars, 5 μm

(Figure 1d), which was consistent with observations using parental HCT116 cells (Figure S1) as well as previous reports (Xie & Pombo, 2006).

We expressed mCherry–PCNA as a marker of replication foci during S phase (Leonhardt et al., 2000) in KI cells to examine the cell cycle dynamics of PCs. Figure 2a shows a typical example representing the dynamics of EGFP–RPB1 and mCherry–PCNA during the cell cycle (Movie S1). A few bright PCs were observed from G_2 to M phase (elapse time, hr:min; 0:00, 2:40 and 3:00). After the mitosis, PCs were

rarely observed during G_1 phase (4:10 and 7:10). The number of PCs increased when the cells entered S phase (7:40, at which mCherry–PCNA was concentrated in many replication foci). Most PCs persisted until the mid to late S phase (13:50 and 16:50) and the number decreased during the G_2 to the next G_1 phase (19:50, 21:50, 22:30 and 26:20). Analysis of 100 cells revealed that the number of PCs per nucleus increased from 0.3 ± 0.5 in G_1 phase (0 in 69% of cells) to 3.0 ± 1.0 in early S phase (3 in 46% of cells) (Figure 2b). It was plausible that PCs appeared in G_1 and S phase are associated with CBs and HLBs that are involved in gene expression of snRNA (expressed in G_1 phase and enhanced in S phase) and histone genes (expressed in S phase) (Faresse et al., 2012; Marzluff & Koreski, 2017; Wang et al., 2016). This prompted us to investigate the relationship between PCs, CBs and HLBs in living cells.

2.2 | Live-cell imaging analysis of the association between PCs, CBs and HLBs

The association between PCs, CBs and HLBs was examined by expressing C-terminally SNAP-tagged coilin (coilin–SNAP) in coilin-KO cells that were generated from KI cells and C-terminally HaloTag-tagged NPAT (NPAT–HaloTag) in KI cells (Figure 1a and Figure S3a–d). Time-lapse imaging (Movie S2) revealed that some PCs nucleated near CBs (~38% of PCs in 75 cells, $n = 232$, Table S2; Figure 3a, arrowhead), whereas the others appeared to be distant from CBs (~62%; Figure 3a, asterisk). The size of PCs was enlarged after association with CBs in some rare cases (~3%, Figure 3a, arrow). In NPAT–HaloTag expressing KI cells, PCs also nucleated near HLBs, but at a higher rate (~51% PCs in 75 cells, $n = 226$, Table S2; Figure 3b, arrowhead; and Movie S3). Some PCs simultaneously formed with HLBs (~25%, Figure 3b, arrow; and Movie S4) while others nucleated away from HLBs (~24%; Figure 3b, asterisk). These observations indicated that PCs preferentially nucleate near or together with HLBs.

We next analyzed how long the PC–CB and PC–HLB associates were maintained using the time-lapse data. The mean association periods were 4.4 ± 1.9 (range, 1.3–9.3) hr for PC–CB ($n = 29$ associates in 22 cells) and 4.6 ± 2.7 (range, 1.0–9.0) hr for PC–HLB ($n = 33$ associates in 22 cells) (Table S3). Most PC–CB (90%) and PC–HLB (76%) associates dissolved within ~6.6 hr of early S phase, as judged from the mCherry–PCNA pattern (Figure 3c). The residual fractions (10% for PC–CB and 24% for PC–HLB) had dissolved by 9.5 hr, before mCherry–PCNA exhibited late-replicating heterochromatic distribution (Figure 3c). PC–CB associates showed four patterns of dissolution: disappearance of PCs in the presence of CBs (38%), disappearance of CBs in the presence of PCs (21%), simultaneous disappearance of both (34%) and separation of a PC–CB associate into two distinct NBs (7%; $n = 29$ associates in 22 cells, Figure 3d and Table S3). PC–HLB associates showed three patterns of dissolution: disappearance of PCs (46%), disappearance of HLBs (12%) and disappearance of both (42%, $n = 33$ associates in 22 cells; Figure 3d and Table S3). These findings indicated that PCs turn over more dynamically than CBs or HLBs.

The relationship between the three NBs (PCs, CBs and HLBs) was examined using live-cell imaging with coilin-KO cells that expressed both coilin–SNAP and NPAT–HaloTag (Figure 1a). These cells showed similar numbers of CBs or HLBs per nucleus to those of parental KI cells (Table S1). PCs in living cells were categorized into four patterns ($n = 382$ PCs in 100 cells; Figure 4a): not associating with CBs or HLBs (17%), associating with only CBs (11%), associating with only HLBs (46%) and associating with both CBs and HLBs (26%). This observation was consistent with the higher rate of PC nucleation nearer HLBs than CBs in the analysis with each combination (Figure 3a,b; Table S2). PC–CB–HLB associates ($n = 142$ in 100 cells imaged for 40 hr) were reverse-tracked to reveal how ternary NB associations were formed. There were three association pathways (Figure 4b,c, pathways A–C; Figure S4; and Movie S5–S7). In more than a half of all cases (53%), PCs and HLBs were simultaneously nucleated near CBs (pathway A; Movie S5). The second major pathway (32%) involved a preformed PC–HLB becoming associated with a nearby CB (pathway B; Movie S6). Nucleation of a PC near a preformed CB–HLB associate (pathway C; Movie S7) was relatively less frequent (15%). These findings are also consistent with PCs preferentially associating with HLBs than with CBs.

2.3 | Coilin-KO did not affect PC formation but affected association between NBs

To investigate the requirement of CBs for PC formation, we used coilin-KO cells, which were generated from KI cells using CRISPR/Cas9 nickase (Figures 1a and 5a,b). Coilin KO did not affect the number (5.4 ± 2.1 and 5.3 ± 1.9 in clones 1 and 2, respectively; Table S1) or phosphorylation status of PCs (Figure S5a). Time-lapse imaging using coilin-KO cells that express mCherry–PCNA revealed that PCs appeared in early S phase (Figure S6a and Movie S8), as observed in KI cells. These data indicate that CBs are not essential for PC formation. Similarly, HLBs and Gems (coilin-negative SMN foci) were still observed in coilin-KO cells, and their numbers were unchanged compared with those of KI cells. By contrast, TCAB1 foci disappeared in coilin-KO cells (Figure S6b and Table S1), supporting an essential role of CBs on TCAB1 foci (Chen et al., 2015; Vogan et al., 2016).

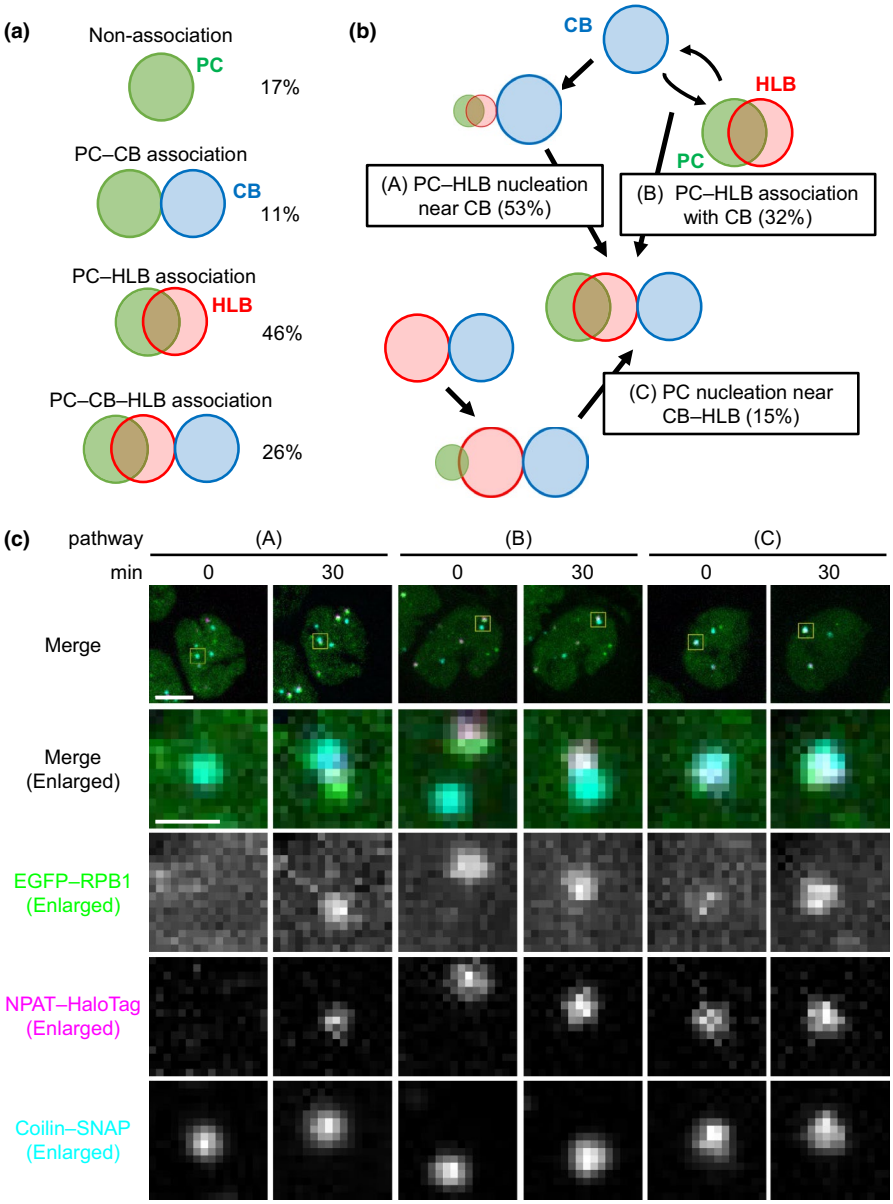

FIGURE 4 Association of NBs in living cells. (a) Association patterns between PCs, CBs and HLBs, based on the analysis of 382 PCs in 100 coilin-KO cells expressing both NPAT–HaloTag and coilin–SNAP. (b) Schematic representation of three assembly pathways of PC–CB–HLB ternary associates. In this analysis, 142 PC–CB–HLB associates in 100 coilin-KO cells expressing both NPAT–HaloTag and coilin–SNAP were reverse-tracked from assembly of the ternary associates using live imaging data for 40 hr. (c) Time-lapse images of EGFP–RPB1 (green), NPAT–HaloTag (JF646; magenta) and coilin–SNAP (TMR; cyan) in coilin-KO cells expressing both NPAT–HaloTag and coilin–SNAP. MIP images of 13 Z-stacks at 0.75 μm intervals are shown. Magnified views of areas indicated by yellow boxes are shown (see Figure S4 for the entire nucleus images). Scale bars, 5 μm; for magnified views, 1 μm

Next, by using immunofluorescence with fixed cells, we analyzed the associations between NBs in KI and coilin-KO cells in more detail. We classified the localization patterns of two protein pairs (i.e., Pol II–coilin, Pol II–NPAT and coilin–NPAT) into three categories: "co-localizing" (most pixels overlapped), "adjacent" (few pixels overlapped) and "nonassociating" (no overlapping pixels) (Figure 5c). Both "co-localizing" and "adjacent" were treated as "associating," which we used in live imaging as the spatial resolution was not high enough to distinguish "co-localizing" from "adjacent." The co-localization rate between HLBs and PCs was higher than that between CBs and PCs in KI cells (Figure 5d and Figure S3d). In coilin-KO cells, HLBs and PCs became more co-localized, while the association between coilin-negative SMN foci (Gems) and PCs decreased (Figure 5d). These data suggest that the associations between PCs and NBs are balanced among different NBs, with a preferred association of PCs with HLBs, and so a PC–HLB association becomes more prominent in the absence of CBs because of a lack of sequestration. By contrast, coilin or CBs may bridge SMN and PCs through the direct interaction between coilin and SMN proteins (Hebert et al., 2001).

We then examined the effect of coilin overexpression on the associations between NBs. In KI cells that overexpressed coilin–SNAP, compared with KI cells, CBs became larger and PCs were more co-localized with CBs (Figure S7) whereas the number of CBs was not substantially increased (Table S4). The co-localization rate of PCs with SMN foci was also increased by coilin–SNAP overexpression (Figure 5d), which was reciprocal to their decreased association in coilin-KO cells (Figure 5d). Coilin–SNAP overexpression did not affect the PC–HLB co-localization rate, again reflecting the preferential association of PCs with HLBs to CBs. These

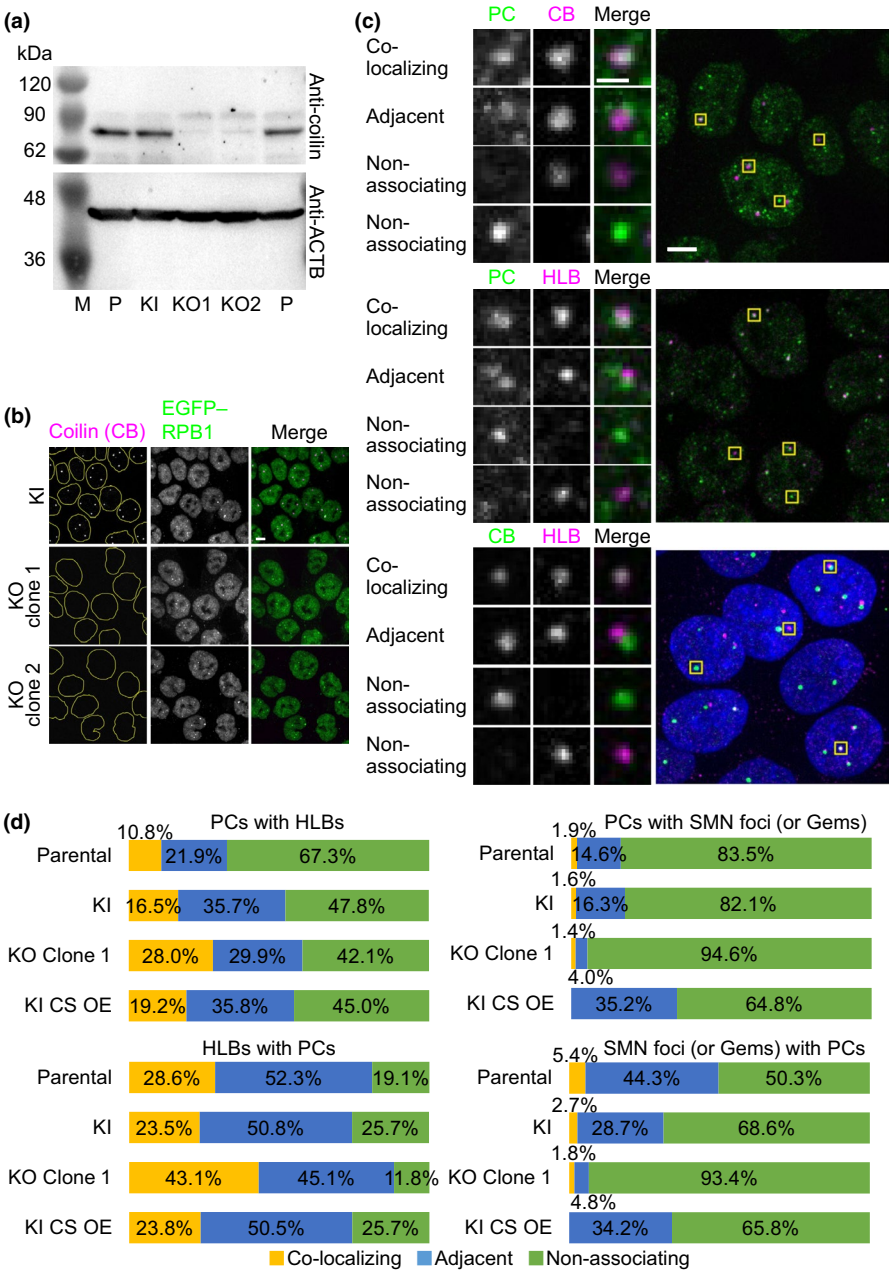

FIGURE 5 Effects of coilin-KO on PC formation and associations with NBs. (a and b) Coilin-KO cells generated by the CRISPR/Cas9 nickase system were analyzed by Western blotting (a) and immunofluorescence (b). (a) Whole-cell lysates separated on an SDS-polyacrylamide gel were probed with antibodies against coilin and ACTB. M, marker; P, parental HCT116 cells; KI, KI cells; KO1, coilin-KO cells clone 1; and KO2, coilin-KO cells clone 2. (b) Immunofluorescence images using antibodies against coilin in KI and coilin-KO cells. All images for coilin (magenta) and EGFP–RPB1 (green) are MIP images of confocal Z-sections to cover the entire nucleus with 0.30 μm intervals (47–57 stacks). Yellow lines indicate nuclear peripheries. (c and d) Association of two heterotopic NBs. (c) Immunofluorescence. KI cells were fixed and stained with antibodies against coilin and NPAT to detect CBs and HLBs, respectively. PCs were detected using EGFP–RPB1. Nuclear DNA was counterstained with Hoechst 33342 (only shown in cells stained with coilin and NPAT; blue). MIP images of Z-stacks at 0.30 μm intervals to cover the entire nucleus (51–58 stacks) are shown. The relationship between two different NBs was classified into three categories: overlapping, adjacent and nonassociating. Magnified views of areas indicated by yellow boxes are shown. Example images are magnified. (d) Association rates between two heterotopic NBs in parental HCT116, KI, coilin-KO clone1 (KO Clone 1) and coilin–SNAP overexpressed KI (KI CS OE) cells. "PCs with HLBs" indicates that the percentage of PCs that were co-localized with, adjacent to, or nonassociated with HLBs (top left). "HLBs with PCs" indicates the percentage of HLBs that were co-localized with, adjacent to or nonassociated with PCs (bottom left). The relationship between PCs and SMN foci, or Gems in coilin KO cells, is indicated on the right. Scale bars, 5 μm; for magnified views, 1 μm

data support the above view that CBs modulate associations between NBs.

As CBs are known to co-localize with CDK7, which phosphorylates Ser5 in the RPB1 CTD (Jordan et al., 1997), the association between PCs and CBs could facilitate Ser5 phosphorylation. However, levels of S5P in PCs with CBs were similar to those in PCs without CBs (Figure S5b,c), suggesting that the function of the PC–CB association is not simply facilitating phosphorylation. In addition, levels of S5P in PCs were also constant, irrespective of the associations with HLBs (Figure S5d). Thus, CBs and HLBs do not appear to play an essential role in regulating Ser5 phosphorylation in PCs.

2.4 | PC depletion did not influence CBs and HLBs

We next investigated the effect of Pol II depletion on CBs and HLBs in parental HCT116 cells using triptolide, which degrades Pol II via RPB1 ubiquitination (Wang et al., 2011). When cells were treated with 5 μM triptolide for 2 hr, Pol II signals detected using anti-CTD antibody were substantially diminished. In contrast, CBs and HLBs remained present in triptolide-treated cells (Figure S8a), and the numbers of CBs and HLBs (average 3.3 and 2.3, respectively) were similar to those with dimethyl sulfoxide (DMSO)-treated control (average 3.4 and 2.2, respectively). The association between CBs and HLBs was also unaffected (Figure S8b). Thus, the integrity of CBs and HLBs was independent of Pol II, consistent with the frequent nucleation of PCs from these NBs, but not vice versa.

2.5 | PCs were liquid-like NBs compared with solid-like CBs and HLBs

Phase-separated NBs exhibit a broad range of biophysical properties, from solid-like to liquid-like (Boeynaems et al., 2018); thus, we investigated the sensitivity of PCs, CBs and HLBs to 1,6-HD, which is known to disrupt liquid-like droplets rather than solid-like materials (Kroschwald et al., 2017). PCs disappeared within 1 min after administration of 1,6-HD, whereas CBs and HLBs remained unchanged in coilin-KO cells expressing coilin–SNAP and KI cells expressing NPAT–HaloTag, respectively (Figure 6), suggesting that PCs had more liquid-like properties compared with CBs and HLBs.

3 | DISCUSSION

The present study analyzed the formation of PCs, CBs and HLBs, and their associations in HCT116 cells. PCs were often nucleated at the beginning of S phase near CBs and HLBs, and PC–CB and PC–HLB associates were dissolved before the end of S phase (Figures 2 and 3; Tables S2 and S3). This observation is consistent with the function of CBs and HLBs, which are localized near sn/snoRNA and/or histone gene clusters and are involved in transcriptional and post-transcriptional regulation of these genes (Wang et al., 2016). CBs were reported to associate with *HIST2* more frequently during late G_1 and S phase compared with other cell cycle phases (Shopland et al., 2001), and HLBs became apparent during S phase (Duronio & Marzluff, 2017). CBs and HLBs can be formed by increased local concentrations of the

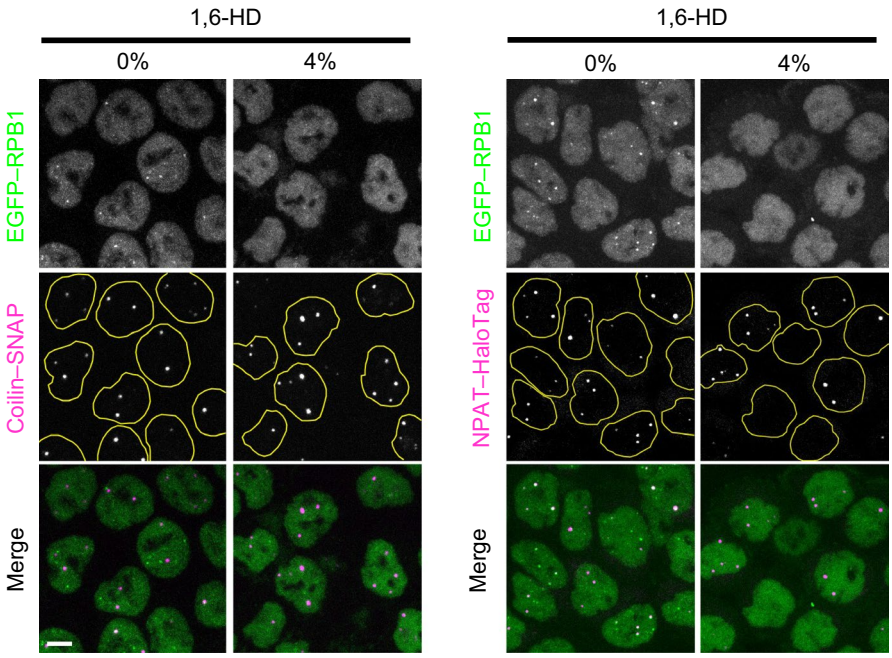

FIGURE 6 1,6-HD only disrupted PCs in living cells. Confocal images of coilin-KO cells expressing coilin–SNAP (left) and KI cells expressing NPAT–HaloTag (right) before and 1 min after the administration of 1,6-HD. MIP images of 11 Z-stacks at 0.90 μm intervals are shown for EGFP–RPB1 (Pol II; green in merge) and coilin–SNAP (CBs) labeled with SNAP–Cell 647–SiR (magenta in merge) or NPAT–HaloTag (HLBs) labeled with Janelia Fluor 646 HaloTag ligand (magenta in merge). Yellow lines indicate nuclear peripheries. Scale bar, 5 μm

component proteins that bind to specific DNA sequence and/or RNA elements at these gene clusters. Once CBs and HLBs are formed, they are quite stably maintained probably because of their rather solid-like droplet nature, relatively resistant to 1,6-HD (Figure S8), through pi/pi, cation/pi and electrostatic interactions (Alberti et al., 2019; Carmo-Fonseca & Rino, 2011; Ghule et al., 2008; Kaiser et al., 2008; Shevtsov & Dundr, 2011). By contrast, PCs were sensitive to 1,6-HD (Figure S8), suggesting their liquid-like nature, which may secure the dynamic turnover of PCs compared with CBs and HLBs. As snRNA and histones are highly transcribed depending on the cell cycle (Faresse et al., 2012; Marzluff & Koreski, 2017; Wang et al., 2016), the formation of PCs near these genes can increase the local concentration of Pol II to facilitate timely transcription. Then, dissolution of PCs may associate with decreased level of transcription.

Cajal bodies and HLBs appear to facilitate the nucleation of PCs near the target gene cluster, such as sn/snoRNA genes (*RNU2* and *SNORD3A*) on chromosome 17 for CBs and the histone gene cluster, *HIST1*, on chromosome 6 for HLBs. Taken together with the fluorescence in situ hybridization data (Wang et al., 2016), the ternary associate of CB, HLB and PC is likely to be formed near chromosome 1 on which both sn/snoRNA genes and histone genes (*RNU1*, *RNU11*, *SNORA72*, *HIST2* and *H3F3A*) are located (Figure 7). A preformed CB on the sn/snoRNA gene locus can act as a core to form a PC–CB–HLB ternary associate via interaction with the histone gene locus, either by stimulating HLB and PC nucleation (Figure 4b,c; pathway A; Figure S4) or interacting with a PC–HLB associate (Figure 4b,c; pathway B; Figure S4). The presence of Pol II harboring S5P and S7P on its CTD in PCs also supports the view that PCs may contribute to the active transcription of sn/snoRNA and histone genes because these phosphorylated forms of Pol II (but not S2P) transcribe these genes (Figure 1d) (Egloff et al., 2007, 2012; Medlin et al., 2005). Although CBs are not essential for the transcription of snRNA and histone genes, as coilin-KO cells grow normally (Lemm et al., 2006; Tucker et al., 2001; Whittom et al., 2008), CBs may contribute to the fine tuning of sn/snoRNA transcription and the formation of other NBs, which may be required for precise developmental regulation (Strzelecka et al., 2010; Tucker et al., 2001; Walker et al., 2009).

Disruption of CBs via coilin KO did not affect PCs in terms of the number per nucleus, nucleation timing and the phosphorylation status of Pol II (Figures S5 and S6; Table S1; Movie S8). However, the association between PCs and HLBs increased in response to coilin KO (Figure 5d). This may be explained by a loss of PC sequestration to CBs. In the absence of CBs, increased free Pol II could facilitate nucleation at HLBs, and/or PCs free of CBs could associate with HLBs. Although it was of interest to investigate the effect of HLB depletion on PCs and CBs, this experiment was not possible in the present study as NPAT is essential for cell cycle progression (Di Fruscio et al., 1997; Ma et al., 2000; Ye et al., 2003). In contrast to the increased association between PCs and HLBs, coilin KO decreased the association between PCs and coilin-negative SMN foci (Gems) (Figure 5d). Reciprocally, coilin–SNAP overexpression, which resulted in increasing the size of CBs, increased the association between PCs and SMN foci (Figure 5d and Table S4). These are consistent with the previous data showing that coilin mediates the interaction between CBs and SMN (Hebert

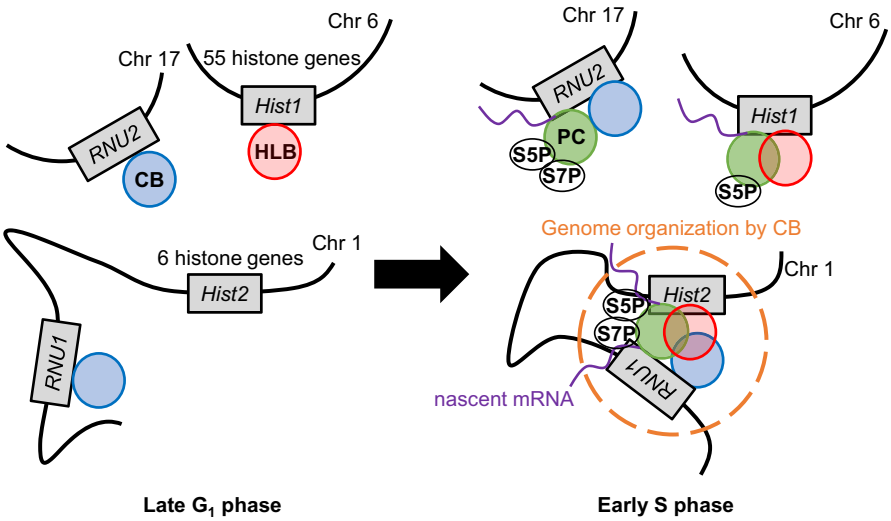

FIGURE 7 A model of the spatiotemporal and functional relationships between PCs, CBs and HLBs. CBs and HLBs can be formed near sn/snoRNA and histone gene clusters with or without PCs. When histone genes are activated in S phase, the number of PCs increases in association with HLBs. CBs can organize histone genes and sn/snoRNA genes on chromosome 1 by forming ternary CB–HLB–PC associates. This genome organization may fine-tune transcription efficiency by Pol II molecules with S5P or S7P CTD in PCs

et al., 2001). Thus, the presence or absence of one type of NB may affect other NBs via direct or indirect associations between NBs. A specific interaction between proteins in different NBs could mediate these associations (Hebert et al., 2001). However, recent studies have suggested that interactions between different NBs may depend more on their biophysical properties than specific protein–protein interactions. Relative surface tensions are considered to be a key parameter in regulating associations between two heterotopic NBs (Bergeron-Sandoval et al., 2016; Feric et al., 2016; Shin & Brangwynne, 2017). Alterations of relative surface tensions among CBs, HLBs and PCs may result in different association patterns. Although we observed overlapping and adjacent associations between NBs, the biological significance of these dynamic interactions remains unclear. Biological surfactant proteins may modulate the interactions between these NBs (Cuylen et al., 2016; Feric et al., 2016).

4 | EXPERIMENTAL PROCEDURES

4.1 | Cell culture, transfection and flow cytometry

HCT116 cells were obtained from ATCC (CCL-247, ATCC) and grown in high-glucose Dulbecco's Modified Eagle Medium (DMEM; 08458-16, NACALAI TESQUE) supplemented with 10% fetal bovine serum (10270-106, Thermo Fisher Scientific), 2 mM L-glutamate, 100 U/ml penicillin and 100 μg/ml streptomycin (G6784-100Ml, Merck, Sigma-Aldrich) under 5% CO_2 at 37°C. Lipofectamine 3000 was used for transfection according to the manufacturer's instructions (L3000015, Thermo Fisher Scientific). Antibiotics selection was carried out by culturing cells in medium supplemented with 500 μg/ml G418 for one week or 2 μg/ml puromycin for two days. A flow cytometer (SH800S, Sony) was used to collect cells expressing fluorescence-tagged proteins.

4.2 | Plasmid construction, genome editing and single-cell cloning

Total RNAs were extracted for use as cDNA synthesis templates using TRIzol (15596026, Thermo Fisher Scientific), treated with RQ1 RNase-Free DNase (M6101, Promega, WI, USA) in the presence of RNaseOUT (10777019, Thermo Fisher Scientific), extracted using phenol/chloroform and precipitated using ethanol according to the manufacturers' instructions. Primers to amplify cDNA were designed using Primer-BLAST (https://www.ncbi.nlm.nih.gov/tools/primer-blast/index.cgi). cDNA was synthesized using a PrimeScript II High Fidelity One Step RT-PCR Kit (R026A, Takara Bio), purified using a QIAquick PCR Purification Kit (QIAGEN, 28106) and cloned into the PiggyBac Transposon Vector (PB533A-2, Funakoshi) or its derivatives with appropriate antibiotics resistant genes (ampicillin for *Escherichia coli* and neomycin or puromycin for mammalian cells) and a tag (SNAP-tag or HaloTag) using an In-Fusion HD Cloning Kit (639635, Takara Bio). The *E. coli* DH5α strain was transformed using In-Fusion products, and single colonies were picked up for plasmid preparation and verification by DNA sequencing. For transfection, plasmids were purified using a Plasmid DNA Midiprep Kit (K210005, Thermo Fisher Scientific).

KI cells were generated by using TALE nuclease (TALEN) knock-in method using a Platinum Gate TALEN Kit, a gift from Takashi Yamamoto (1000000043, Addgene) (Sanjana et al., 2012). To construct a TALEN pair that targets the 1st exon of POLR2A, DNA-binding modules for 5′-ATGCACGGGGGT-3′ and 5′-GCATGCGCTGTC-3′ were assembled into the ptCMV–153/47 vector, respectively. To construct a donor vector (pDonor–EGFP–POLR2A), ~1,000 bp upstream of the annotated start codon of POLR2A, EGFP with A206K mutation, ~250 bp fragment of the 1st exon including coding sequence, loxP-puromycin selection marker-loxP, and ~1,000 bp of downstream sequence were tandemly flanked by PCR and inserted into the pBlueScript vector. The TALEN plasmids and pDonor–EGFP–POLR2A were co-transfected into parental HCT116 cells by electroporation using an NEPA21 super electroporator (Nepa Gene). Puromycin-resistant clones were isolated and validated by genomic PCR, DNA sequencing and Western blotting. Note that KI cells used in this study spontaneously lost the puromycin cassette at the loxP site for unknown reasons.

Coilin-KO cells were generated using the Cas9 nickase system (pX335 and pKN7; Addgene) (Cong et al., 2013) with single guide RNAs designed using CHOPCHOP (http://chopchop.cbu.uib.no/). KO of the coilin gene (*COIL*) was achieved using the following sequences: 5′-TGCCTCAGGTGCGCGGCGCA<u>GGG</u>-3′ (forward) and 5′-TCCGCGCGCGAGAGCCGCCC<u>CCC</u>-3′ (reverse), where the PAM sequence is underlined.

For single-cell cloning, transfected cells were resuspended in DMEM, filtered through a 40 μm cell strainer (352340, Corning), and seeded at a density of 1,000 cells/20 ml in a 15-cm dish. After incubation in a CO_2 incubator for a week, single colonies were picked using a P20 pipette tip under a conventional phase–contrast microscope and transferred to an ibidi-coated 96-well plate (μ-Plate 96 Well Black, 89626, ibidi).

4.3 | Antibodies, dyes, florescent ligands and chemicals

All antibodies, dyes and florescent ligands are listed in Table S5. Three mouse α-RPB1 CTD monoclonal

antibodies (IgGs) were generated in our laboratory (Stasevich et al., 2014). The mouse monoclonal α-CTD antibody (C13B9) was generated using the unphosphorylated synthetic peptide corresponding to the CTD heptarepeat; however, the antibody can also recognize phosphorylated CTD (Stasevich et al., 2014). Fab preparation and dye-conjugation were carried out as previously described (Hayashi-Takanaka et al., 2011; Stasevich et al., 2014). 1,6-HD was purchased from Tokyo Chemical Industry (H0099, Tokyo, Japan), dissolved in DMEM, filtered through a 0.2 μm filter for sterilization and stored at 4°C. Triptolide was purchased from Tocris Bioscience (3253, Tocris, R&D Systems), dissolved in DMSO at 100 μM and stored at −30°C. Triptolide was diluted in cell culture medium immediately prior to use.

4.4 | Immunofluorescence, live-cell imaging and image analysis

All immunofluorescence procedures were carried out at room temperature. Cells were fixed in 4% paraformaldehyde, 0.1% Triton X-100 and 250 mM HEPES, pH 7.4 for 20 min, rinsed three times in Dulbecco's phosphate-buffered saline (D-PBS) (−) (048-29805, FUJIFILM Wako Pure Chemical) and permeabilized with 1% Triton X-100 in D-PBS (−) for 20 min. After blocked with Blocking One P (05999-84, NACALAI TESQUE) for 20 min and rinsed in D-PBS (−), the processed cells were incubated with primary antibodies in D-PBS (−) for 2 hr. Cells were rinsed three times in D-PBS (−), incubated with secondary antibodies and Hoechst 33342 (H3570, Thermo Fisher Scientific) in D-PBS (−) for 2 hr and rinsed three times in D-PBS (−).

For live-cell imaging, cells were seeded on ibidi-treated culture dishes (μ-Slide 8 Well, 80826, or μ-Dish 35 mm high, 81156, ibidi) and cultured for one to two days. The medium was replaced with FluoroBright (A1896701, Thermo Fisher Scientific) containing 10% fetal bovine serum, 2 mM L-glutamate, 100 U/ml penicillin and 100 μg/ml streptomycin, immediately prior to imaging. Images were acquired using a spinning disk confocal microscope comprising an inverted microscope (Ti-E, Nikon), a Plan-Apo VC 100× (NA 1.4) oil immersion objective lens (NA 1.4; with Type F immersion oil, MXA22168, Nikon), a spinning disk unit (CSU-W1, Yokogawa), an EM-CCD camera (iXon3 DU888 X-8465, Andor) and a LU-N4 laser unit (Nikon) under the control of an operating software (NIS-Elements, Nikon). Live-cell imaging was carried out at 37°C under 5% of CO_2 using a stage top incubator (INUBG2TF-WSKM-A14R, Tokai-Hit). Images were analyzed using Icy (Chaumont et al., 2012) (http://icy.bioimageanalysis.org/). Individual Z-section images were used for quantitative analysis, although Max-Intensity-Projection (MIP) images of Z-series were presented in all figures unless stated otherwise. To detect foci of NBs, the threshold was set as 30 percentiles intensity to cut off pixels with intensity <30% of an intensity histogram of all pixels in an image with a size filer between 10 and 150 pixels in order. All results were checked visually and, in cases in which 30 percentiles did not sufficiently detect foci, the threshold value was changed manually. The distance threshold judged as "co-localizing" was within 3 pixels (390 nm) between centers of foci in 3D. We analyzed cells that exhibited at least one PC, CB, HLB, SMN focus or TCAB1 focus.

4.5 | Western blotting

Cells were trypsinized, collected into 15-ml tubes and washed twice in 10 ml PBS (−). The cell density was counted and lysed in Laemmli buffer without dithiothreitol and bromophenol blue to yield 1×10^7 cells/ml. Whole-cell lysates were heated at 95°C for 10 min and stored at −30°C. Protein concentration was measured using a bicinchoninic acid assay kit (297-73101, FUJIFILM Wako Pure Chemical). After supplemented with dithiothreitol and bromophenol blue, and boiling at 95°C for 5 min, whole lysates (50 μg to detect coilin or 90 μg to detect RPB1 and GFP) were separated by sodium dodecyl sulfate (SDS)-polyacrylamide gel electrophoresis (90 min at 20 mA constant currency per 85 mm height gel). Gels were gently shaken in Transfer buffer (100 mM Tris, 200 mM glycine and 5% methanol) for 10 min. Polyvinylidene fluoride membranes (BSP0161, FluoroTrans W PVDF Transfer Membranes, Pall, NY, USA) were immersed in methanol for 3 min and equilibrated in Transfer buffer for 10 min with gentle shaking. Proteins on gels were transferred to membranes for 60 min at 150 mA (for coilin) or 250 mA (for RPB1) per 85 × 90 mm membrane. After an incubation in Blocking One (03953-95, NACALAI TESQUE) for 20 min with gentle shaking, membranes were incubated with primary antibodies diluted in Can Get Signal Solution I (NKB-101, TOYOBO) overnight at 4°C (for coilin and GFP) or 2 hr at room temperature (for RPB1). After washed in TBS-T (100 mM Tris-HCl, pH 8.0, 0.1% Tween-20, 150 mM NaCl) for 20 min three times, membranes were incubated with horseradish peroxidase-conjugated secondary antibodies (80 ng/ml, AB_10015289, Jackson ImmunoResearch) in Can Get Signal Solution II (NKB-101, TOYOBO) for 1 hr at room temperature. After membranes were washed in TBS-T for 20 min three times, signals were developed using ImmunoStar LD (296-69901, FUJIFILM Wako Pure Chemical) and detected using a gel documentation system (LuminoGraph II, ATTO).

ACKNOWLEDGEMENTS

This work was in part of supported by MEXT/JSPS KAKENHI (JP17H01417 and JP18H05527 to H.K.; JP18H05498 to Y.S.) and Japan Science and Technology Agency (JST) CREST JPMJCR16G1 to H.K. We thank the member of Kimura lab for constructive discussion and the Biomaterials Analysis Division, Open Facility Center, Tokyo Institute of Technology for DNA sequencing analysis. We are grateful to Yoshida Scholarship Foundation for financial support to T.I during his PhD program.

CONFLICT OF INTEREST

The authors declare that there are no conflicts of interest.

ORCID

Takashi Imada http://orcid.org/0000-0001-9283-3787
Takeshi Shimi https://orcid.org/0000-0002-9864-1820
Yasushi Saeki https://orcid.org/0000-0002-9202-5453
Hiroshi Kimura https://orcid.org/0000-0003-0854-083X

REFERENCES

Alberti, S., Gladfelter, A., & Mittag, T. (2019). Considerations and challenges in studying liquid-liquid phase separation and biomolecular condensates. *Cell*, *176*, 419–434. https://doi.org/10.1016/j.cell.2018.12.035

Alm-Kristiansen, A. H., Saether, T., Matre, V., Gilfillan, S., Dahle, Ø., & Gabrielsen, O. S. (2008). FLASH acts as a co-activator of the transcription factor c-Myb and localizes to active RNA polymerase II foci. *Oncogene*, *27*, 4644–4656. https://doi.org/10.1038/onc.2008.105

Bergeron-Sandoval, L., Safaee, N., & Michnick, S. W. (2016). Mechanisms and consequences of macromolecular phase separation. *Cell*, *165*, 1067–1079. https://doi.org/10.1016/j.cell.2016.05.026

Boehning, M., Dugast-Darzacq, C., Rankovic, M., Hansen, A. S., Yu, T., Marie-Nelly, H., McSwiggen, D. T., Kokic, G., Dailey, G. M., Cramer, P., Darzacq, X., & Zweckstetter, M. (2018). RNA polymerase II clustering through carboxy-terminal domain phase separation. *Nature Structural & Molecular Biology*, *25*, 833–840. https://doi.org/10.1038/s41594-018-0112-y

Boeynaems, S., Alberti, S., Fawzi, N. L., Mittag, T., Polymenidou, M., Rousseau, F., Schymkowitz, J., Shorter, J., Wolozin, B., Van Den Bosch, L., Tompa, P., & Fuxreiter, M. (2018). Protein phase separation: a new phase in cell biology. *Trends in Cell Biology*, *28*, 420–435. https://doi.org/10.1016/j.tcb.2018.02.004

Carmo-Fonseca, M., & Rino, J. (2011). RNA seeds nuclear bodies. *Nature Cell Biology*, *13*, 110–112. https://doi.org/10.1038/ncb0211-110

Cauchi, R. J. (2010). SMN and gemins: 'We Are Family' … or are we? *BioEssays*, *32*, 1077–1089. https://doi.org/10.1002/bies.201000088

Chapman, R. D., Palancade, B., Lang, A., Bensaude, O., & Eick, D. (2004). The last CTD repeat of the mammalian RNA polymerase II large subunit is important for its stability. *Nucleic Acids Research*, *32*, 35–44. https://doi.org/10.1093/nar/gkh172

Chen, Y., Deng, Z., Jiang, S., Hu, Q., Liu, H., Songyang, Z., Ma, W., Chen, S., & Zhao, Y. (2015). Human cells lacking coilin and cajal bodies are proficient in telomerase assembly, trafficking and telomere maintenance. *Nucleic Acids Research*, *43*, 385–395. https://doi.org/10.1093/nar/gku1277

Cong, L., Ran, F. A., Cox, D., Lin, S., Barretto, R., Habib, N., & Zhang, F. (2013). Multiplex genome engineering using CRISPR/Cas systems. *Science*, *339*, 819–823. https://doi.org/10.1126/science.1231143

Cuylen, S., Blaukopf, C., Politi, A. Z., Müller-Reichert, T., Neumann, B., Poser, I., & Gerlich, D. W. (2016). Ki-67 acts as a biological surfactant to disperse mitotic chromosomes. *Nature*, *535*, 308–312. https://doi.org/10.1038/nature18610

de Chaumont, F., Dallongeville, S., Chenouard, N., Hervé, N., Pop, S., Provoost, T., Meas-Yedid, V., Pankajakshan, P., Lecomte, T., Le Montagner, Y., Lagache, T., Dufour, A., & Olivo-Marin, J.-C. (2012). Icy: An open bioimage informatics platform for extended reproducible research. *Nature Methods*, *9*, 690–696. https://doi.org/10.1038/nmeth.2075

Di Fruscio, M., Weiher, H., Vanderhyden, B. C., Imai, T., Shiomi, T., Hori, T. A., & Gray, D. A. (1997). Proviral inactivation of the Npat gene of Mpv 20 mice results in early embryonic arrest. *Molecular and Cellular Biology*, *17*, 4080–4086. https://doi.org/10.1128/mcb.17.7.4080

Duronio, R. J., & Marzluff, W. F. (2017). Coordinating cell cycle-regulated histone gene expression through assembly and function of the histone locus body. *RNA Biology*, *14*, 726–738. https://doi.org/10.1080/15476286.2016.1265198

Egloff, S., O'Reilly, D., Chapman, R. D., Taylor, A., Tanzhaus, K., Pitts, L., & Murphy, S. (2007). Serine-7 of the RNA Polymerase II CTD is specifically required for SnRNA gene expression. *Science*, *318*, 1777–1779. https://doi.org/10.1126/science.1145989

Egloff, S., Zaborowska, J., Laitem, C., Kiss, T., & Murphy, S. (2012). Ser7 phosphorylation of the CTD recruits the RPAP2 Ser5 phosphatase to SnRNA genes. *Molecular Cell*, *45*, 111–122. https://doi.org/10.1016/j.molcel.2011.11.006

Faresse, N. J., Canella, D., Praz, V., Michaud, J., Romascano, D., & Hernandez, N. (2012). Genomic study of RNA polymerase II and III SNAPc-bound promoters reveals a gene transcribed by both enzymes and a broad use of common activators. *PLOS Genetics*, *8*, e1003028. https://doi.org/10.1371/journal.pgen.1003028

Feric, M., Vaidya, N., Harmon, T. S., Mitrea, D. M., Zhu, L., Richardson, T. M., & Brangwynne, C. P. (2016). Coexisting liquid phases underlie nucleolar subcompartments. *Cell*, *165*, 1686–1697. https://doi.org/10.1016/j.cell.2016.04.047

Frey, M. R., & Matera, A. G. (2001). RNA-mediated interaction of Cajal bodies and U2 SnRNA genes. *Journal of Cell Biology*, *154*, 499–510. https://doi.org/10.1083/jcb.200105084

Ghule, P. N., Dominski, Z., Yang, X., Marzluff, W. F., Becker, K. A., Harper, J. W., & Stein, G. S. (2008). Staged assembly of histone gene expression machinery at subnuclear foci in the abbreviated cell cycle of human embryonic stem cells. *Proceedings of the National Academy of Sciences of the United States of America*, *105*, 16964–16969. https://doi.org/10.1073/pnas.0809273105

Guglielmi, B., Rochelle, N. L., & Tjian, R. (2013). Gene-specific transcriptional mechanisms at the histone gene cluster revealed by single-cell imaging. *Molecular Cell*, *51*, 480–492. https://doi.org/10.1016/j.molcel.2013.08.009

Guo, Y. E., Manteiga, J. C., Henninger, J. E., Sabari, B. R., Dall'Agnese, A., Hannett, N. M., Spille, J. H., Afeyan, L. K., Zamudio, A. V., Shrinivas, K., Abraham, B. J., Boija, A., Decker, T. M., Rimel, J. K., Fant, C. B., Lee, T. I., Cisse, I. I., Sharp, P. A., Taatjes, D. J., & Young, R. A. (2019). Pol II phosphorylation regulates a switch between transcriptional and splicing condensates. *Nature*, *572*, 543–548. https://doi.org/10.1038/s41586-019-1464-0

Harlen, K. M., & Churchman, L. S. (2017). The code and beyond: Transcription regulation by the RNA polymerase II carboxy-terminal domain. *Nature Reviews Molecular Cell Biology*, *18*, 263–273. https://doi.org/10.1038/nrm.2017

Hayashi-Takanaka, Y., Yamagata, K., Wakayama, T., Stasevich, T. J., Kainuma, T., Tsurimoto, T., Tachibana, M., Shinkai, Y., Kurumizaka, H., Nozaki, N., & Kimura, H. (2011). Tracking epigenetic histone modifications in single cells using fab-based live endogenous modification labeling. *Nucleic Acids Research*, *39*, 6475–6488. https://doi.org/10.1093/nar/gkr343

Hebert M. D., Szymczyk, P. W., Shpargel, K. B., & Matera, A. G. (2001). Coilin forms the bridge between Cajal bodies and SMN, the Spinal Muscular Atrophy protein. *Genes & Development*, *15*(20), 2720–2729. http://dx.doi.org/10.1101/gad.908401

Henriksson, S., & Farnebo, M. (2015). On the road with WRAP53β: Guardian of Cajal bodies and genome integrity. *Frontiers in Genetics*, *6*, 91. https://doi.org/10.3389/fgene.2015.00091

Jordan, P., Cunha, C., & Carmo-Fonseca, M. (1997). The Cdk7-Cyclin H-MAT1 complex associated with TFIIH is localized in coiled bodies. *Molecular Biology of the Cell*, *8*, 1207–1217. https://doi.org/10.1091/mbc.8.7.1207

Kaiser, T. E., Intine, R. V., & Dundr, M. (2008). De novo formation of a subnuclear body. *Science*, *322*, 1713–1717. https://doi.org/10.1126/science.1165216

Kim, W. Y., & Dahmus, M. E. (1989). The major late promoter of adenovirus-2 is accurately transcribed by RNA polymerases IIO, IIA, and IIB. *Journal of Biological Chemistry*, *264*, 3169–3176. https://doi.org/10.1016/S0021-9258(18)94046-9

Klingauf, M., Staněk, D., & Neugebauer, K. M. (2006). Enhancement of U4/U6 small nuclear ribonucleoprotein particle association in cajal bodies predicted by mathematical modeling. *Molecular Biology of the Cell*, *17*, 4972–4981. https://doi.org/10.1091/mbc.E06-06-0513

Kroschwald, S., Maharana, S., & Simon, A. (2017). Hexanediol: A chemical probe to investigate the material properties of membraneless compartments. *Matters*, *3*, e201702000010. https://doi.org/10.19185/matters.201702000010

Lamond, A. I., & Carmo-Fonseca, M. (1993). The coiled body. *Trends in Cell Biology*, *3*, 198–204. https://doi.org/10.1016/0962-8924(93)90214-l

Lemm, I., Girard, C., Kuhn, A. N., Watkins, N. J., Schneider, M., Bordonné, R., & Lührmann, R. (2006). Ongoing U SnRNP biogenesis is required for the integrity of Cajal bodies. *Molecular Biology of the Cell*, *17*, 3221–3231. https://doi.org/10.1091/mbc.e06-03-0247

Leonhardt, H., Rahn, H. P., Weinzierl, P., Sporbert, A., Cremer, T., Zink, D., & Cardoso, M. C. (2000). Dynamics of DNA replication factories in living cells. *Journal of Cell Biology*, *149*, 271–280. https://doi.org/10.1083/jcb.149.2.271

Liu, Q., & Dreyfuss, G. (1996). A novel nuclear structure containing the survival of motor neurons protein. *The EMBO Journal*, *15*, 3555–3565. https://doi.org/10.1016/S0021-9258(18)94046-9

Lu, H., Yu, D., Hansen, A. S., Ganguly, S., Liu, R., Heckert, A., & Zhou, Q. (2018). Phase-separation mechanism for C-terminal hyperphosphorylation of RNA Polymerase II. *Nature*, *558*, 318–323. https://doi.org/10.1038/s41586-018-0174-3

Ma, T., Tine, B. A. V., Wei, Y., Garrett, M. D., Nelson, D., Adams, P. D., & Harper, J. W. (2000). Cell cycle-regulated phosphorylation of P220(NPAT) by cyclin E/Cdk2 in Cajal bodies promotes histone gene transcription. *Genes & Development*, *14*, 2298–2313. https://doi.org/10.1101/gad.829500

Machyna, M., Neugebauer, K. M., & Staněk, D. (2015). Coilin: The first 25 years. *RNA Biology*, *12*, 590–596. https://doi.org/10.1080/15476286.2015.1034923

Maita, H., & Nakagawa, S. (2020). What Is the Switch for coupling transcription and splicing? RNA Polymerase II C-terminal domain phosphorylation, phase separation and beyond. *Wires RNA*, *11*, e1574. https://doi.org/10.1002/wrna.1574

Marzluff, W. F., Gongidi, P., Woods, K. R., Jin, J., & Maltais, L. J. (2002). The human and mouse replication-dependent histone genes. *Genomics*, *80*, 487–498. https://doi.org/10.1006/geno.2002.6850

Marzluff, W. F., & Koreski, K. P. (2017). Birth and death of histone mRNAs. *Trends in Genetics*, *33*, 745–759. https://doi.org/10.1016/j.tig.2017.07.014

Medlin, J., Scurry, A., Taylor, A., Zhang, F., Peterlin, B. M., & Murphy, S. (2005). P-TEFb is not an essential elongation factor for the intronless human U2 SnRNA and histone H2b genes. *EMBO Journal*, *24*, 4154–4165. https://doi.org/10.1038/sj.emboj.7600876

Nizami, Z. F., Deryusheva, S., & Gall, J. G. (2010a). Cajal bodies and histone locus bodies in Drosophila and Xenopus. *Cold Spring Harbor Symposia on Quantitative Biology*, *75*, 313–320. https://doi.org/10.1101/sqb.2010.75.005

Nizami, Z., Deryusheva, S., & Gall, J. G. (2010b). The Cajal body and histone locus body. *Cold Spring Harbor Perspectives in Biology*, *2*, a000653. https://doi.org/10.1101/cshperspect.a000653

Raimer, A. C., Gray, K. M., & Matera, A. G. (2016). SMN - A chaperone for nuclear RNP social occasions? *RNA Biology*, *14*, 701–711. https://doi.org/10.1080/15476286.2016.1236168

Romeo, V., & Schümperli, D. (2016). Cycling in the nucleus: Regulation of RNA 3' processing and nuclear organization of replication-dependent histone genes. *Current Opinion in Cell Biology*, *40*, 23–31. https://doi.org/10.1016/j.ceb.2016.01.015

Sanjana, N. E., Cong, L., Zhou, Y., Cunniff, M. M., Feng, G., & Zhang, F. (2012). A Transcription Activator-Like Effector (TALE) toolbox for genome engineering. *Nature Protocols*, *7*, 171–192. https://doi.org/10.1038/nprot.2011.431

Sawyer, I. A., Sturgill, D., & Dundr, M. (2019). Membraneless nuclear organelles and the search for phases within phases. *Wires RNA*, *10*, e1514. https://doi.org/10.1002/wrna.1514

Sawyer, I. A., Sturgill, D., Sung, M., Hager, G. L., & Dundr, M. (2016). Cajal body function in genome organization and transcriptome diversity. *BioEssays*, *38*, 1197–1208. https://doi.org/10.1002/bies.201600144

Schul, W., Driel, R., & Jong, L. (1998). Coiled bodies and U2 SnRNA genes adjacent to coiled bodies are enriched in factors required for SnRNA transcription. *Molecular Biology of the Cell*, *9*, 1025–1036. https://doi.org/10.1091/mbc.9.5.1025

Shevtsov, S. P., & Dundr, M. (2011). Nucleation of nuclear bodies by RNA. *Nature Cell Biology*, *13*, 167–173. https://doi.org/10.1038/ncb2157

Shin, Y., & Brangwynne, C. P. (2017). Liquid phase condensation in cell physiology and disease. *Science*, *357*, https://doi.org/10.1126/science.aaf4382

Shopland, L. S., Byron, M., Stein, J. L., Lian, J. B., Stein, G. S., & Lawrence, J. B. (2001). Replication-dependent histone gene expression is related to Cajal Body (CB) association but does not require sustained CB contact. *Molecular Biology of the Cell*, *12*, 565–576. https://doi.org/10.1091/mbc.12.3.565

Sleeman, J. E., Trinkle-Mulcahy, L., Prescott, A. R., Ogg, S. C., & Lamond, A. I. (2003). Cajal body proteins SMN and coilin show

differential dynamic behaviour in vivo. *Journal of Cell Science*, *116*, 2039–2050. https://doi.org/10.1242/jcs.00400

Staněk, D. (2017). Cajal bodies and SnRNPs - Friends with benefits. *RNA Biology*, *14*, 671–679. https://doi.org/10.1080/15476286.2016.1231359

Staněk, D., & Fox, A. H. (2017). Nuclear bodies: News insights into structure and function. *Current Opinion in Cell Biology*, *46*, 94–101. https://doi.org/10.1016/j.ceb.2017.05.001

Stasevich, T. J., Hayashi-Takanaka, Y., Sato, Y., Maehara, K., Ohkawa, Y., Sakata-Sogawa, K., Tokunaga, M., Nagase, T., Nozaki, N., McNally, J. G., & Kimura, H. (2014). Regulation of RNA Polymerase II activation by histone acetylation in single living cells. *Nature*, *516*, 272–275. https://doi.org/10.1038/nature13714

Steurer, B., Janssens, R. C., Geverts, B., Geijer, M. E., Wienholz, F., Theil, A. F., Chang, J., Dealy, S., Pothof, J., van Cappellen, W. A., Houtsmuller, A. B., & Marteijn, J. A. (2018). Live-cell analysis of endogenous GFP-RPB1 uncovers rapid turnover of initiating and promoter-paused RNA Polymerase II. *Proceedings of the National Academy of Sciences of the United States of America*, *115*, E4368–E4376. https://doi.org/10.1073/pnas.1717920115

Strom, A. R., & Brangwynne, C. P. (2019). The liquid nucleome - phase transitions in the nucleus at a glance. *Journal of Cell Science*, *132*, jcs235093. https://doi.org/10.1242/jcs.235093

Strzelecka, M., Trowitzsch, S., Weber, G., Lührmann, R., Oates, A. C., & Neugebauer, K. M. (2010). Coilin-dependent SnRNP assembly is essential for zebrafish embryogenesis. *Nature Structural & Molecular Biology*, *17*, 403–409. https://doi.org/10.1038/nsmb.1783

Tucker, K. E., Berciano, M. T., Jacobs, E. Y., LePage, D. F., Shpargel, K. B., Rossire, J. J., Chan, E. K. L., Lafarga, M., Conlon, R. A., & Matera, A. G. (2001). Residual Cajal bodies in coilin knockout mice fail to recruit Sm SnRNPs and SMN, the spinal muscular atrophy gene product. *Journal of Cell Biology*, *154*, 293–308. https://doi.org/10.1083/jcb.200104083

Uversky, V. N. (2017). Intrinsically disordered proteins in Overcrowded Milieu: Membrane-less organelles, phase separation, and intrinsic disorder. *Current Opinion in Structural Biology*, *44*, 18–30. https://doi.org/10.1016/j.sbi.2016.10.015

Venteicher, A. S., Abreu, E. B., Meng, Z., McCann, K. E., Terns, R. M., Veenstra, T. D., Terns, M. P., & Artandi, S. E. (2009). A Human telomerase holoenzyme protein required for Cajal body localization and telomere synthesis. *Science*, *323*, 644–648. https://doi.org/10.1126/science.1165357

Vogan, J. M., Zhang, X., Youmans, D. T., Regalado, S. G., Johnson, J. Z., Hockemeyer, D., & Collins, K. (2016). Minimized human telomerase maintains telomeres and resolves endogenous roles of H/ACA proteins, TCAB1, and Cajal bodies. *Elife*, *5*, e18221. https://doi.org/10.7554/eLife.18221

Walker, M. P., Tian, L., & Matera, A. G. (2009). Reduced viability, fertility and fecundity in mice lacking the Cajal body marker protein, Coilin. *PLoS One*, *4*, e6171. https://doi.org/10.1371/journal.pone.0006171

Wang, Q., Sawyer, I. A., Sung, M.-H., Sturgill, D., Shevtsov, S. P., Pegoraro, G., Hakim, O., Baek, S., Hager, G. L., & Dundr, M. (2016). Cajal bodies are linked to genome conformation. *Nature Communication*, *7*, 10966. https://doi.org/10.1038/ncomms10966

Wang, Y., Lu, J., He, L., & Yu, Q. (2011). Triptolide (TPL) inhibits global transcription by inducing proteasome-dependent degradation of RNA Polymerase II (Pol II). *PLoS One*, *6*, e23993. https://doi.org/10.1371/journal.pone.0023993

Whittom, A. A., Xu, H., & Hebert, M. D. (2008). Coilin levels and modifications influence artificial reporter splicing. *Cellular and Molecular Life Sciences*, *65*, 1256–1271. https://doi.org/10.1007/s00018-008-7587-3

Xie, S. Q., & Pombo, A. (2006). Distribution of different phosphorylated forms of RNA Polymerase II in relation to Cajal and PML bodies in human cells: An Ultrastructural Study. *Histochemistry and Cell Biology*, *125*, 21–31. https://doi.org/10.1007/s00418-005-0064-2

Ye, X., Wei, Y., Nalepa, G., & Harper, J. W. (2003). The cyclin E/Cdk2 substrate p220NPAT is required for S-Phase entry, histone gene expression, and Cajal body maintenance in human somatic cells. *Molecular and Cellular Biology*, *23*, 8586–8600. https://doi.org/10.1128/MCB.23.23.8586-8600.2003

SUPPORTING INFORMATION

Additional supporting information may be found online in the Supporting Information section.

How to cite this article: Imada T, Shimi T, Kaiho A, Saeki Y, Kimura H. RNA polymerase II condensate formation and association with Cajal and histone locus bodies in living human cells. *Genes Cells*. 2021;26: 298–312. https://doi.org/10.1111/gtc.12840